

Feature-based Terrain Editing From Complex Sketches

Flora Ponjou Tasse^{a,*}, Arnaud Emilien^{b,c}, Marie-Paule Cani^b, Stefanie Hahmann^b, Neil Dodgson^a

^aUniversity of Cambridge

^bLaboratoire Jean Kuntzmann (Univ. Grenoble-Alpes, CNRS) and Inria

^cLIGUM, Dept. I.R.O., Montreal University

Abstract

We present a new method for first person sketch-based editing of terrain models. As in usual artistic pictures, the input sketch depicts complex silhouettes with cusps and T-junctions, which typically correspond to non-planar curves in 3D. After analysing depth constraints in the sketch based on perceptual cues, our method best matches the sketched silhouettes with silhouettes or ridges of the input terrain. A deformation algorithm is then applied to the terrain, enabling it to exactly match the sketch from the given perspective view, while insuring that none of the user-defined silhouettes is hidden by another part of the terrain. We extend this sketch-based terrain editing framework to handle a collection of multi-view sketches. As our results show, this method enables users to easily personalize an existing terrain, while preserving its plausibility and style.

Keywords: First person editing, terrain, sketch-based modelling, silhouettes

1. Introduction

Terrain is a key element in any outdoor environment. Applications of virtual terrain modelling are very common in movies, video games, advertisement and simulation frameworks such as flight simulators. Two of the most popular terrain modelling methods are procedural [1, 2, 3, 4] and physics-based techniques [4, 5, 6, 7, 8, 9]. The former are easy to implement and fast to compute, while the latter produce terrains with erosion effects and geologically sound features. However, the lack of controllability in these methods is a limitation for artists.

Sketch-based or example-based terrains have been popular recently in addressing these issues [10, 11, 12, 13, 14, 15, 16]. However, many of these methods [12, 14, 16] assume that the user sketch is drawn from a top view, which makes shape control from a viewpoint of interest difficult. Others [10, 11, 13, 15] only handle a restricted category of mountains, with flat silhouettes. Lastly, terrains fully generated from sketches typically lack details. Dos Passos et al. [17] recently presented a promising approach where example-based terrain modelling and a first person point-of-view sketch are combined. However their method does not support local terrain editing and cannot handle typical terrain silhouettes with T-junctions. Moreover, terrain patches are often repeated which may spoil the plausibility of the results from other viewpoints.

In this work, we address the problem of intuitive shape control of a terrain from a first person viewpoint, while generating detailed output that is plausible from any viewpoint. To achieve the intuitive shape control goal, we stick to the sketch-based approach, but allow the user to input complex silhouettes, as those are typically used to represent terrains (see Figure 1).

Our interpretation of the term “complex” is similar to the one used in SmoothSketch [18], where a complex sketch is a set of 2D strokes with hidden contours and cusps. To get plausible, detailed results from any viewpoint, we focus on editing an existing terrain rather than starting from scratch. This approach captures the coherent small details from the existing terrain, while avoiding the patch blending and repetition problems that are typical of example-based methods. The use of an existing terrain also enables matches of sketched silhouettes with plausible, non planar curves on the terrain.

In practice, the user edits the input terrain by over-sketching it from a first person viewpoint. The user strokes, forming a graph of curves with T-junctions, represent the desired silhouettes for the terrain. The input terrain is then deformed such that its silhouettes exactly match the strokes in the current perspective view. This means that each stroke segment is to be some silhouette of the output terrain, and that no other part of the deformed terrain should hide them. Previous sketch-based modelling methods have successfully use feature curves to deform surfaces [19, 20]. Our work explores the use of terrain features for sketch-based terrain editing.

Paper contributions. This paper is an extended version of earlier work [21] in which we first introduced a framework for deforming terrain features to fit user strokes. First, sketched strokes are ordered by inferring their relative depth from the height of their end-points and from the T-junctions detected in the sketch. Next, features of the input terrain such as silhouette edges and ridges are assigned to each stroke and extended if necessary, to cover the length of the stroke. This assignment is the solution of a minimization problem expressing the similarity between a terrain feature and a stroke in the drawing plane, and the amount of deformation caused by their matching. The selected features then become constraints for an it-

*e-mail:flora.ponjou-tasse@cl.cam.ac.uk

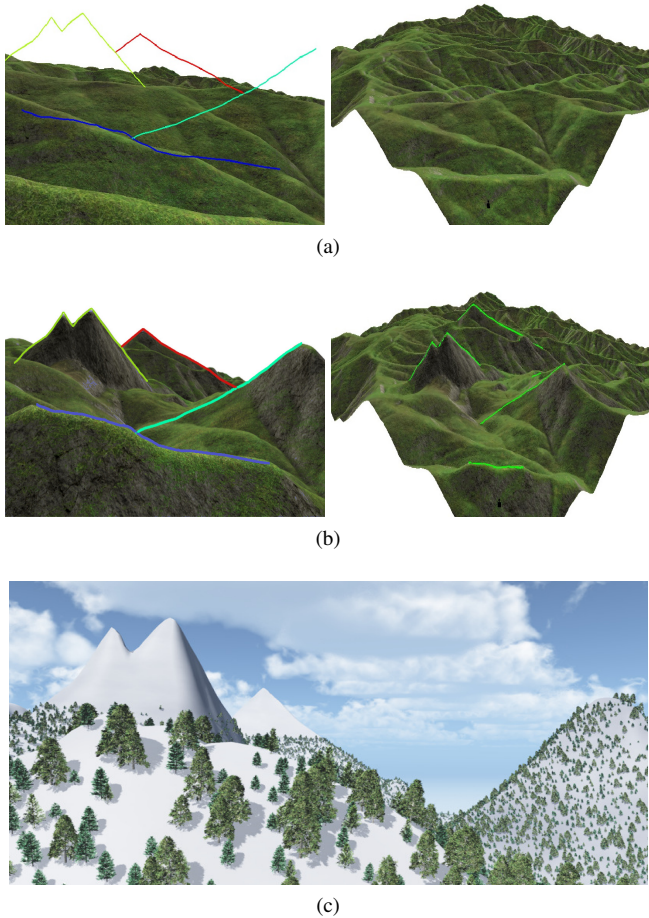


Figure 1: (a) An artist sketch (left), is used to edit an existing terrain (right). (b) Results shown from two viewpoints. Note the complex silhouettes with T-junctions, matched to features of the input terrain. (c) shows a rendering of the resulting terrain, from a closer viewpoint.

64 erative diffusion-based terrain deformation method. The main
 65 contributions of that earlier paper [21] are:

- 66 • An algorithm for ordering strokes in a complex, perspec-
 67 tive sketch with respect to their distance from the camera.
- 68 • A method for matching terrain features with user-specified
 69 silhouettes, drawn from a given first-person viewpoint.
- 70 • A deformation method for matching silhouette constraints
 71 while preventing them from being hidden by other parts
 72 of the terrain.

73 This paper provides an in-depth discussion of the branch-
 74 and-bound search scheme used to address the energy minimiza-
 75 tion problem. Additionally, we propose an improved frame-
 76 work that supports terrain editing from multi-view sketches drawn
 77 from different viewpoints. In the context of film making, this
 78 additional tool can facilitate control of the exact shape of ter-
 79 rain silhouettes for two or three views, which will be used for
 80 key scenes. Although iteratively editing the terrain from mul-
 81 tiple viewpoints could achieve realistic landscapes, there is no
 82 guarantee that silhouettes generated during one iteration will
 83 not be significantly modified by subsequent iterations. The

84 stroke-to-feature matching algorithm is modified to handle all
 85 sketches at once, with additional constraints that ensure that no
 86 assigned feature is occluded by another. Finally, we claimed
 87 in the original paper that specifically deforming terrain features
 88 produces more realistic results. To illustrate this, we compare
 89 the use of feature-based curve constraints in terrain deforma-
 90 tion against using 3D planar curve constraints obtained from
 91 projecting strokes on the drawing plane. We show how the two
 92 types of constraints affect terrain deformation and realism on 3
 93 different test cases.

94
 95 We begin by summarising related work (Section 2). We
 96 then give an overview of our whole system (Section 3), be-
 97 fore describing, in detail, stroke ordering (Section 4), feature
 98 constraints (Section 5), terrain deformation (Section 6), and the
 99 modifications needed to handle multi-view sketches from vari-
 100 ous viewpoints (Section 7).

101 2. Related work

102 Most terrain modelling systems use one or a combination
 103 of the following: procedural terrain generation, physics-based
 104 simulation, sketch-based or example-based methods. Natali et
 105 al. [22] provide a detailed survey.

106 Procedural terrain modelling methods are based on the fact
 107 that terrains are self-similar, i.e. statistically invariant under
 108 magnification. Fractals have the same concept of self-similarity
 109 [23] and thus, fractal-based methods have been widely used in
 110 terrain generation. These methods are the popular choice for
 111 landscape modelling due to their easy implementation and ef-
 112 ficient computation. They mainly consist of pseudo-randomly
 113 editing height values on a flat terrain by using either adaptive
 114 subdivision [1, 2, 3] or noise [2, 4]. Adaptive subdivision pro-
 115 gressively increases the level of detail of the terrain by itera-
 116 tively interpolating between neighbouring points and displac-
 117 ing the new intermediate points by increasingly smaller random
 118 values. Noise synthesis techniques are often preferred because
 119 they offer better control. Superposing scaled-down copies of a
 120 band-limited, stochastic noise function generates noise-based
 121 terrains. For more information on fractal terrain generation
 122 methods, see Ebert et al. [24]. Fractal-based approaches can
 123 generate a wide range of large terrains with unlimited level of
 124 details. However, they are limited by the lack of user con-
 125 trol or non-intuitive parameter manipulation, and the absence
 126 of erosion effects such as drainage patterns. To address the
 127 last issue, fractal terrains can be improved using physics-based
 128 erosion simulation [4, 5, 6, 7, 8, 9]. Alternatively, river net-
 129 work generation can be incorporated in the procedural method
 130 [25, 16]. In particular, Genevaux et al. [16] create procedu-
 131 ral terrains from a hydrographically and geomorphologically
 132 consistent river drainage network, generated from a top-view
 133 sketch. However, this method only captures terrains resulting
 134 from hydraulic erosion, and there is no mechanism for control-
 135 ling their silhouettes from a first person viewpoint.

136
 137 Physically-based techniques generate artificial terrains by
 138 simulating erosion effects over some input 3D model. Mus-

grave et al. [4] present the first methods for thermal and hydraulic erosion based on geomorphology rules. Roudier et al. [5] introduce a hydraulic erosion simulation that uses different materials at various locations resulting in different interactions with water. Chiba et al. [6] generate a vector field of water flow that then controls how sediment moves during erosion. This process produces hierarchical ridge structures and thus enhances realism. Nagashima [7] combines thermal and fluvial erosion by using a river network pre-generated with a 2D fractal function. Neidhold et al. [8] present a physically correct simulation based on fluids dynamics and interactive methods that enable the input of global parameters such as rainfall or local water sources. Kristof et al. [9] propose fast hydraulic erosion based on Smooth Particle Hydrodynamics. The main drawback of all these methods is that they only allow indirect user-control through trial and error, requiring a good understanding of the underlying physics, time and efforts to get the expected results.

Sketching interfaces and more generally feature-based editing have been increasingly popular for terrain modelling. These methods can be combined with some input terrain data to generate terrains with plausible details.

Cohen et al. [10] and Watanabe et al. [11] present the first terrain modelling interfaces that take as input a 2D silhouette stroke directly drawn on a 3D terrain model. They only handle a single silhouette stroke, interpreted as a flat feature curve. McCrae and Singh [26] use stroke-based input to create paths which deform terrains. However user strokes are interpreted as path layouts and not as terrain silhouettes. Multi-grid diffusion methods enable generation of terrains that simultaneously match several feature curves, either drawn from a top view [14] or from an arbitrary viewpoint [27]. The main limitation is that generated terrains typically lack realistic details.

In contrast, Zhou et al. [12] use features (actually, sketch maps painted from above) to drive patch-based terrain synthesis from real terrain data. Closer to our concerns, Gain et al. [13] deform an existing terrain from a set of sketched silhouettes and boundary curves. The algorithm deforms the terrain based on the relative distance to the feature-curves in their region of influence, and on wavelet noise to add details to the silhouettes. In this work we rather use a diffusion-based deformation method to propagate feature constraints, avoiding the need for boundary curves. Lastly, Tasse et al. [15] present a distributed texture-based terrain generation method that re-uses the same sketching interface. Unfortunately, all these methods interpret each sketched silhouette as a planar feature curve, which reduces the realism of the result.

Dos Passos et al. [17] propose a different approach to address this issue. Given a set of sketched strokes drawn from a first person point-of-view, copies of an example terrain are combined such that the silhouettes of the resulting terrain match the strokes. This gives a realistic, varying depth to silhouettes. To achieve this, the algorithm assumes each stroke represents a terrain silhouette. A stroke is matched with a portion of a silhouette, selected from a set of silhouettes viewed from several standing viewpoints around the example terrain. Terrain

slices representing portions of matched silhouette are cut from the example terrain and then combined through a weighted sum to produce a smooth terrain. A drawback of this method is that it does not handle complex sketches with T-junctions, which are common in landscape drawings. Moreover, the matching process may select the same silhouette portions for different strokes, thus producing unrealistic repeating patterns in the final result. Finally, the weighted sum function used for merging may fail to remove the boundary seams produced by combining different terrain slices. In this work, we address these issues by presenting a sketch-based method that handles T-junctions in complex sketches and deforms an input terrain to match the sketch rather than copy-pasting parts of it.

3. Overview

Let us describe our processing pipeline. As in many terrain modelling and rendering methods, our terrains are represented by a *height field*, implemented as a greyscale image storing elevation values. This representation cannot emulate features such as overhangs and caves, but it is the most prevalent format in terrain generation because of its simplicity and efficient use of storage space. For rendering purposes and silhouette detection, a 3D triangular mesh is constructed from the height field by connecting adjacent terrain points $(x, y, altitude(x, y))$. Users are able to navigate on a 3D rendering of the existing terrain, possibly flat, with a first-person camera always at a standing viewpoint. A sketch is created by drawing one or multiple strokes from the same camera position. The drawn strokes represent silhouettes that the artist wishes to be visible from that position. Our main goal is to deform the terrain such that these user constraints are respected. The following requirements should be satisfied:

- Every sketched stroke should be a terrain silhouette, in the current perspective view from the first-person camera viewpoint.
- Each of these terrain silhouettes should be visible, i.e. not hidden by any other part of the terrain.
- The deformed terrain should not have artifacts nor contain unrealistic deformations, from any other viewpoint.

Our solution consists of five steps, illustrated in Figure 2.

Stroke ordering: We order strokes according to their depth, from front to back with respect to the camera position. This order is used when we generate constraints for terrain deformation, so that a curve constraint is not occluded by another, when viewed from the first-person viewpoint.

Feature detection: Terrain features such as silhouettes and ridges are detected. Deforming existing terrain features to match the desired silhouettes results in a more realistic terrain since no extra features are added and thus, the nature of the existing terrain is best preserved.

Stroke-feature matching: For each stroke, we select a terrain feature that will be deformed to fit the stroke, when seen from the camera position. These deformed features represent

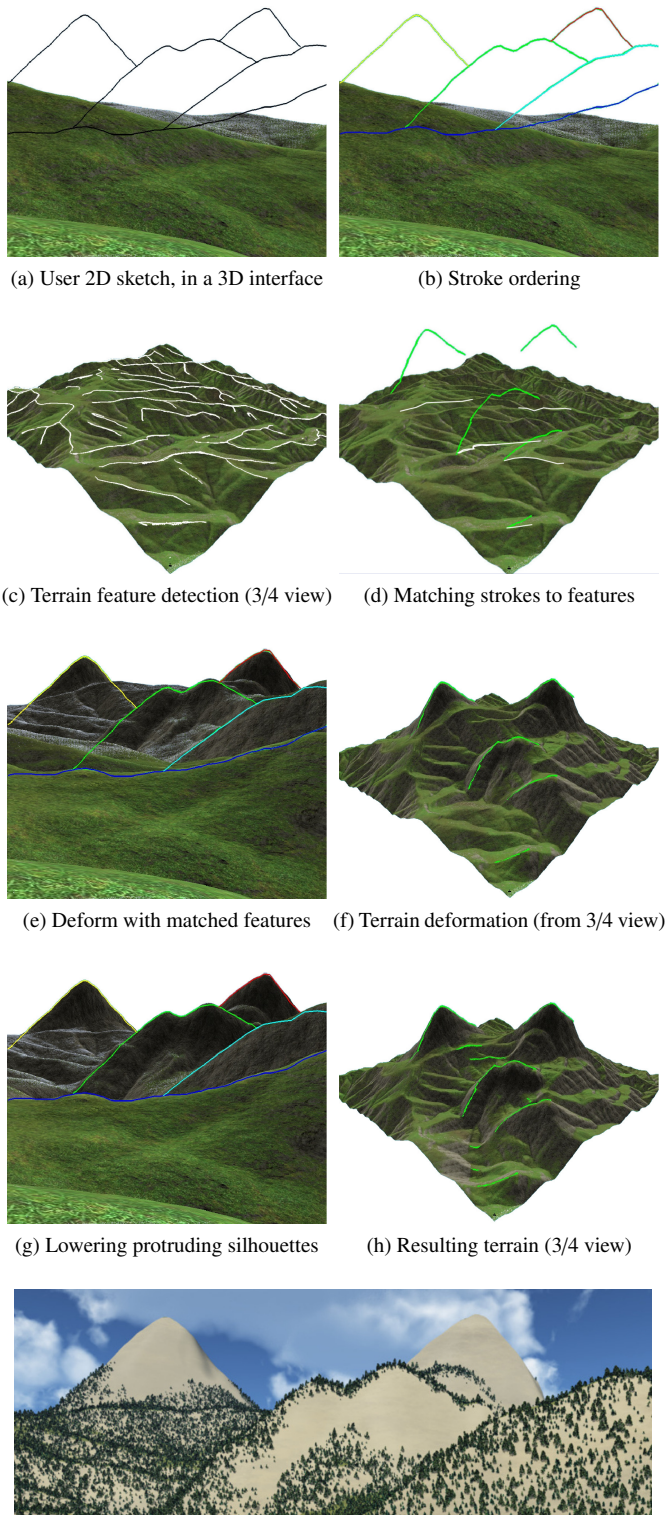


Figure 2: Overview of our terrain editing framework. (a) Unlabeled user sketch. In (b), stroke colour indicates stroke ordering: blue indicates that a stroke is closer to the camera position and red indicates that it is the furthest. (c) illustrates detected features in white and (d) shows the subset of features that are assigned to user strokes. In (e,f) the terrain features are deformed so that they match the strokes from the user viewpoint. The final result in (g,h) is obtained after removing some residual artifacts.

248 the positional constraints that we use in the diffusion-based ter-
 249 rain deformation. A key idea of our framework is the expres-
 250 sion of this feature selection step as an energy minimization
 251 problem, in which we penalize features with large altitude dif-
 252 ferences compared to their corresponding stroke as well as fea-
 253 tures that would result in too large deformations.

254 **Terrain deformation:** We use a multi-grid Poisson solver
 255 for diffusion-based terrain deformation. It solves for altitude
 256 differences instead of absolute terrain positions, thus preserving
 257 the small-scale features of the input terrain.

258 **Lowering protruding silhouettes:** After terrain deforma-
 259 tion, other parts of the terrain may hide the user-specified sil-
 260 houettes. To address this issue, we run the following iterative
 261 process: we detect terrain silhouettes that do not fit any user
 262 stroke and yet hide one of the sketched silhouettes. Extra de-
 263 formation constraints are constructed to enforce lowering these
 264 protruding silhouettes until the user-sketched silhouettes are no
 265 longer occluded. The terrain is deformed with a combination of
 266 previous constraints and the newly constructed constraints. We
 267 repeat this process until there is no longer protruding silhouette.

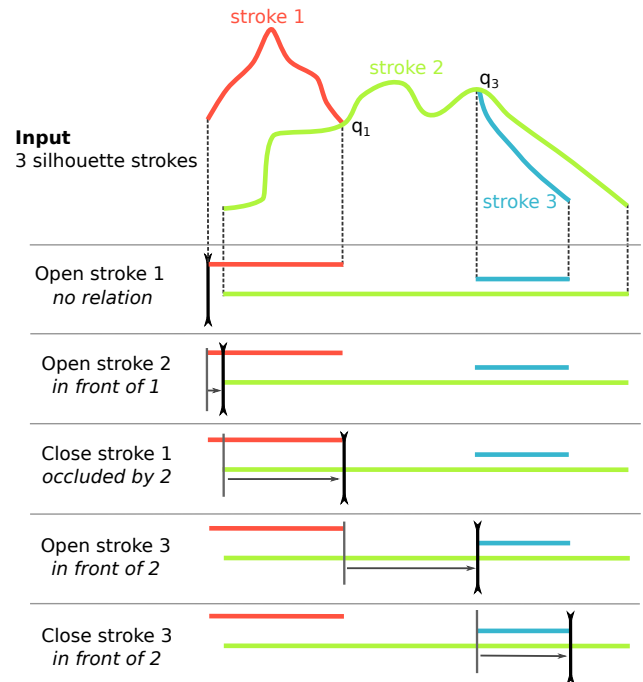


Figure 3: An input sketch (top) and the different steps of the sweeping algorithm used for scanning the sketch, labelling T-junctions and ordering strokes (bottom). As a result, stroke 3 is detected to be in front of stroke 2, which is itself in front of stroke 1. Note that the stroke colouring at the top is for illustration purposes only, the input sketch being unlabeled.

268 4. Analysing complex terrain sketches

269 In this section, we explain how depth ordering of silhouette
 270 strokes is extracted from the user sketch.

271 The different silhouette strokes in the input sketch first need
 272 to be ordered, in terms of relative depth from the camera view-
 273 point. This is necessary since the input strokes are not labeled
 274 and thus there no information of the order in which they should

275 be processed. This will enable us to ensure, when they are
 276 matched with features, that they will not be hidden by other
 277 parts of the terrain. Our approach to do so is based on two ob-
 278 servations:

- 279 • If, in the viewing plane, a silhouette lies above another, it
 280 obviously corresponds to a mountain A farther away from
 281 the viewpoint than the other mountain B . Otherwise A
 282 would hide B . Using height coverage for ordering them
 283 in depth is however not sufficient, since some strokes may
 284 overlap in height, as for the green and blue strokes in
 285 Figure 3.
- 286 • Furthermore, the terrain being a height field, the projec-
 287 tion of each stroke onto the horizon (x -axis of the view-
 288 ing plane) is injective (no more than one height value per
 289 point).

290 These two observations allow us to solve the relative stroke
 291 ordering problem using our new sweeping algorithm (see Fig-
 292 ure 3): We consider the projections of all the strokes onto the
 293 horizontal x axis (depicted in the bottom part of the Figure)
 294 and sweep from left to right, examining the extremities (start-
 295 ing and endpoints in sweeping direction) and junction points of
 296 the silhouette strokes. While doing so, we label the strokes’
 297 extremities and the junction points in the following way: an ex-
 298 tremity q_s of stroke s is a T-junction if its closest distance to an-
 299 other stroke r is smaller than a threshold. Information about the
 300 junction point of two strokes is used to unambiguously decide
 301 which stroke is occluded and thus, further from to the camera.
 302 An endpoint q_s is labelled (*occluded-by*, r) if the oriented an-
 303 gle, measured counterclockwise, between the tangent¹ of s at q_s
 304 and the tangent of r at q_s , $\angle(t_s, t_r) < 180^\circ$. This indicates that s
 305 is occluded by, and thus behind, r . Otherwise, s is in front of r
 306 and we label q_s as (*in-front-of*, r).

307 In the absence of T-junctions, stroke ordering is determined
 308 using the height values at extremities. First, we check if once
 309 both strokes are projected on the horizontal axis, the interval
 310 $[r_{right}, r_{left}]$ is a subset of $[s_{right}, s_{left}]$. If this is the case, we say
 311 that the projection of s completely contains the projection of r
 312 and s is behind r . Otherwise, the stroke with the lowest height
 313 is considered closer to the camera and thus, s is behind r if the
 314 smallest height value of s ’s endpoints is larger than the smallest
 315 height value of r ’s endpoints.

316 While scanning the sketch from left to right, we insert each
 317 stroke in a sorting structure, at a relative depth position deter-
 318 mined by the cues above. This results in a relative ordering of
 319 the user strokes.

320 5. Positioning strokes in world space

321 The key idea of our approach is to create a 3D terrain that
 322 matches the user drawing, by deforming an existing one. More

323 precisely, we deform the features of the existing terrain, like its
 324 ridge lines, to match the user silhouette strokes. Because a ter-
 325 rain has many features, we first have to compute to which one of
 326 them it is the most appropriate to apply a deformation. In this
 327 section, we detail how we compute the set of terrain features
 328 (Section 5.1), how we allocate one of them to each of the user
 329 strokes (Section 5.2) and we present a feature completion algo-
 330 rithm that infers the hidden parts of the silhouettes, enabling a
 331 more realistic terrain deformation result (Section 5.3).

332 5.1. Feature detection: silhouettes and ridgelines

333 Silhouette detection on the existing terrain is based on a
 334 common and naive algorithm for computing the exact silhou-
 335 ettes of a 3D mesh. Silhouette edges are detected by finding all
 336 visible edges shared by a front face and a back face in the cur-
 337 rent perspective view. Neighbouring silhouette edges are then
 338 linked to form long silhouette curves.

339 Ridge detection is based on the profile-recognition and polygon-
 340 breaking algorithm (PPA) by Chang et al. [28]. The PPA algo-
 341 rithm marks each terrain point that is likely to be on a ridge line,
 342 based on the point height profile. Segments, forming a cyclic
 343 graph, connect adjacent candidate points. Polygon-breaking re-
 344 peatedly deletes the lowest segment in a cycle until the graph
 345 is acyclic. Finally, the branches on the produced tree structure
 346 are reduced and smoothed. The result is a graph where nodes
 347 are end points or branch points connected by curvilinear ridge-
 348 lines. An improvement of the PPA algorithm connects all the
 349 terrain points into a graph using a height-based or curvature-
 350 based weighting and computes the minimum spanning tree of
 351 that graph [29]. Because we are mainly concerned with perfor-
 352 mance and detection of large-scale ridges, we simply connect
 353 candidate terrain points as in the original PPA algorithm and
 354 replace the polygon-breaking with a minimum spanning forest
 355 algorithm.

357 5.2. Stroke - Feature matching

358 In this section, we discuss a method for determining, for
 359 each stroke, the terrain features which can be used to construct
 360 deformation curve constraints. Viewed from the first person
 361 camera, these curve constraints should match the user-sketched
 362 strokes. To achieve this, we first construct a feature priority
 363 list for each stroke and then select features for each priority list
 364 such that the sum of their associated cost is minimized.

365 5.2.1. Feature priority list per stroke

366 For a stroke s , we project all terrain features on the sketch-
 367 ing plane (i.e. we use the 2D projection of the feature from the
 368 first-person viewpoint) and select feature curves that satisfy the
 369 following condition: the x interval they cover matches the one
 370 of the stroke s . We deform the selected feature curves, and
 371 if necessary extend their endpoints, such that viewed from the
 372 camera position, they cover the length of s . This deformation is
 373 simply achieved by displacing the feature curve points accord-
 374 ing to their projection on the 2D stroke in the sketching plane,
 375 and their distance to the camera position. Let f be a terrain fea-
 376 ture and f_p its projection on the stroke plane. We sweep s from

¹Strokes are always oriented clockwise. Hence, stroke tangents are inde-
 pendent of the direction in which the stroke was sketched. When labelling a
 starting point q_s as T-junction, we flip its tangent.

377 one extremity to another with a vertical line and sections of f
 378 whose projection on f_p never intersect this line are removed.
 379 Moreover, for each point $q \in f$, its altitude is modified as fol-
 380 lows:

$$381 \quad q.z = q.z + k \|q_p - q_p^s\| \frac{\|q - p_c\|}{\|q_p - p_c\|}$$

382 where p_c is the camera position, $k = -1$ if f_p is below s and
 383 $k = 1$ otherwise, q_p the projection of q on the stroke plane, and
 384 q_p^s the intersection of s and the vertical line passing at q_p .

385 We used this deformed version of the feature to associate the
 386 following cost $E(f, s)$ to each feature f with respect to stroke s :

$$387 \quad E = E_{\text{dis}} + E_{\text{def}} + E_{\text{sam}} + E_{\text{ext}} \quad (1)$$

$$E_{\text{dis}}(f) = \frac{w_1}{\text{CurveLength}(f_p)} \int_{f_p} h_{f_p} dt$$

$$E_{\text{def}}(f) = \frac{w_2}{\text{CurveLength}(f)} \int_f h_f dt$$

$$E_{\text{sam}}(f) = \frac{w_3 \times \text{LongestEdgeLength}(f)}{\max_{g \in \text{list}(s)} \text{LongestEdgeLength}(g)}$$

$$E_{\text{ext}}(f) = \frac{w_4 \times \text{ExtendedCurveLength}(f)}{\text{CurveLength}(f)}$$

388 where w_i are weights, f_p is the projection of f on the stroke
 389 plane, h_f is the altitude difference between f and f_p 's projec-
 390 tion on the terrain, and h_{f_p} is the altitude difference between f_p
 391 and the stroke s . The cost E_{dis} represents the dissimilarity be-
 392 tween f and s , E_{def} expresses the amount of deformation along
 393 f , E_{sam} penalizes features with long edges and E_{ext} penalizes
 394 features that were extended to fully cover s when viewed from
 395 the camera position. All the results shown here were generated
 396 with $w_1 = w_2 = w_3 = w_4 = 1.0$.

397 All features are sorted in a priority list according to their
 398 cost. Figure 4 illustrates this process for a single stroke (in this
 399 simple case, the feature of minimal cost is selected).

400 5.2.2. Energy minimization

401 The goal here is the selection of a feature curve f from
 402 the priority list of each stroke s_i , to construct deformation con-
 403 straints for terrain deformation. In addition to the feature order
 404 within the different priority lists, we need to take into account
 405 the depth ordering for silhouette strokes computed in Section 4.

406 Therefore, this selection process can be seen as a minimiza-
 407 tion problem. We want to find a set of stroke-feature matches
 408 such that the total cost of the assignments is minimized and the
 409 assigned features respect the pre-computed stroke ordering. Let
 410 $S = \{s_i : i = 1, \dots, n\}$ be the stroke list (ordered by depth) and f^i
 411 denote a feature in the priority list $L(s_i) = \{f_k^i : k = 1, \dots, m_i\}$ for
 412 a stroke s_i . We are looking for $\{f^i : i \in 1 \dots n\}$ such that $f^i < f^j$
 413 if $i < j$ and $\sum E(f^i)$ is minimized. Here, $f^i < f^j$ means that f^i
 414 should not be occluded by f^j , so that all deformation curve con-
 415 straints are visible from the first person viewpoint. We process
 416 the ordered stroke list from front to back, and after each stroke,
 417 we remove from the priority list of the next strokes, features
 418 that will be occluded if selected. We chose to process strokes

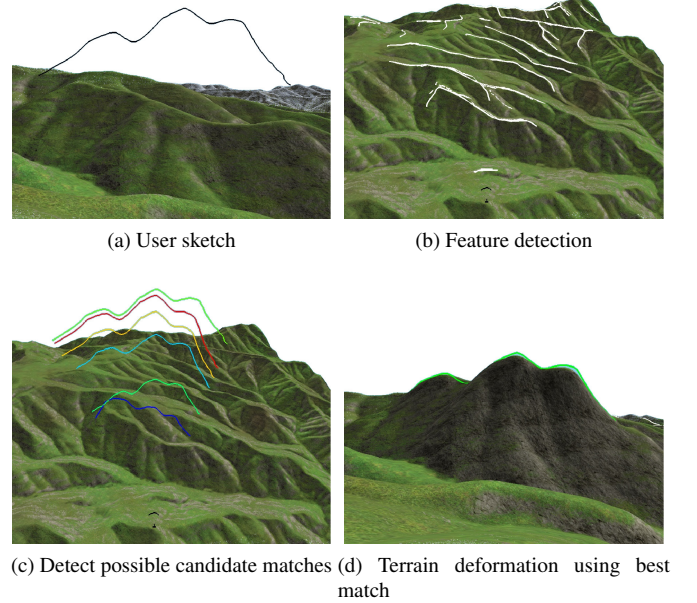


Figure 4: Computing possible features to match with a user stroke. Images (a) and (d) show the terrain from the first person viewpoint used for editing, while image (b) and (c) use a higher viewpoint to better show features on the input terrain. Feature colour indicates cost: blue for the lowest cost and red for the highest.

419 from front to back for two main reasons. Firstly, strokes that
 420 are closest to the eye are processed first and due to E_{def} , the
 421 algorithm attempts to select constraints that will minimize the
 422 terrain deformation. Thus, features closer to the eye are more
 423 likely to be selected. Secondly, if all the features of interest for
 424 a given stroke s_i were already selected, and therefore its priority
 425 list was empty, an arbitrary curve on the terrain would be used
 426 instead. If this ever occurs, we prefer it to be for background
 427 silhouettes.

428 In practice, feature selections that cause any stroke to have
 429 an empty priority list are penalized with a very high cost. Thus,
 430 a configuration that guarantees at least one valid feature match
 431 for each stroke is always selected, if it exists. If no such config-
 432 uration exists and s_i has an empty priority list, we automatically
 433 compute a 3D embedding of the 2D stroke s_i and use the result-
 434 ing curve as a deformation constraint. To easily compute this
 435 3D embedding, we take the two strokes lying just in front and
 436 just behind s_i . Then we place s_i halfway between the terrain
 437 features assigned to these two strokes. If there is no stroke re-
 438 stricted to lie behind s_i , we place it behind the furthest stroke
 439 from the viewpoint. If there is no stroke restricted to lie in front
 440 of s_i , we place it in front of the closest stroke to the viewpoint.
 441 With this approach, each stroke is represented by a deformation
 442 constraint even if it was not matched to a terrain feature during
 443 the energy minimization.

444 The energy minimization problem we have described so far
 445 is a NP-hard combinatorial optimization problem. Branch-and-
 446 bound approaches are often used to overcome such computa-
 447 tionally expensive exhaustive searches [30], since they are de-

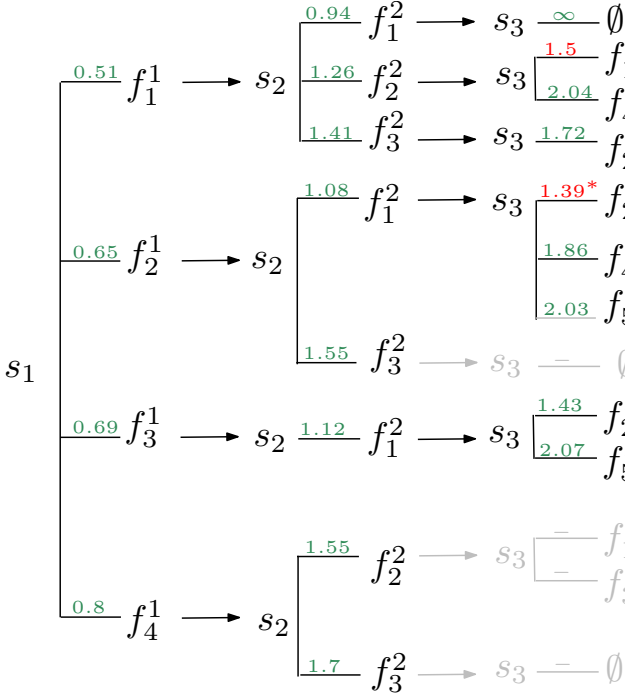


Figure 5: Energy minimization. We use a branch and bound search scheme to find the best stroke-feature matching that minimizes the total cost. Each stroke (in this example, s_1, s_2, s_3) has a priority list of potential candidate features, ordered from the most to the least preferable. Here s_1 has four candidates, s_2 has three and s_3 has five. Note how assigning one feature to a stroke often invalidates some features for subsequent strokes. Moreover, if a stroke no longer has a valid feature it can be assigned to, the corresponding branch has an infinite cost. Once a solution is found, branches that are guaranteed to have a cost higher than the current optimal solution are not explored (indicated in gray). The asterisk (*) indicates the current best solution.

signed to discard non-optimal solutions early on. Here, we use the branch-and-bound scheme to efficiently discard all partial solutions that have a cost higher than the current best cost, without having to explore the whole solution tree. The algorithm consists of two steps: a *branching* step and a *bounding* step. The branching step consists of exploring possible choices for s_{i+1} once we have made a feature selection for s_i . In other words, we split the node (s_i, f^i) into multiple nodes (s_{i+1}, f_k^{i+1}) , where f_k^{i+1} are features in the priority list of s_{i+1} . The bounding step allows the algorithm to stop exploring a partial solution if the total cost of features in the solution is higher than the cost of the best solution found so far. Figure 5 illustrates the search for an optimal solution, given a sketch with 3 strokes.

It is possible for a feature to be the first choice in the priority lists for two or more strokes. To handle this, when exploring a possible solution, a feature curve assigned to a stroke is no longer considered for subsequent strokes. Our branch and bound algorithm will explore other solutions with the feature curve assigned to different strokes as long these solutions are guaranteed to have a smaller cost than the current best solution.

5.2.3. Stroke in world space

The previous minimization gives us, for each stroke s , an associated terrain feature f . However, the stroke s has its points in screen space, whereas the points of f are in the world space.

Our goal is to place the stroke in the world space, in order to deduce terrain constraints, i.e. find the distance of their projection from the camera.

For each point of the stroke $q_s = (x_s, y_s)$, we check if there exists a feature point q_f whose projection on screen $q_p = P(q_f) = (x_p, y_p)$ has the same x-coordinate as q_s , i.e. $x_s = x_p$. If this point exists, we project the stroke point on the world space, using the distance of q_f from the camera as a depth value.

The possible undetermined points depth, at the stroke borders, are set in world space to follow the stroke tangent, in the world space.

5.3. Completing selected 3D features

Using user-specified endpoints of an occluded stroke during the generation of deformation constraints would create silhouettes that appear to start exactly at these endpoints. This can look quite unnatural when viewed from a different position than the first person camera position used for sketching: indeed, the endpoint of the occluded stroke (a junction) is typically above the terrain and thus, a sharp deformation will be created at that point.

We address this problem by extending 3D features assigned to strokes at both endpoints along their tangents, until they reach the surface of the terrain. This is provided as an optional step in the editing process. An example of feature completion is presented in Figure 6. This simple approach only produces realistic terrain silhouettes for strokes with a low-frequency structure. More sophisticated contour completion methods such as the one presented in SmoothSketch [18] could alternatively be used to support elaborate strokes.

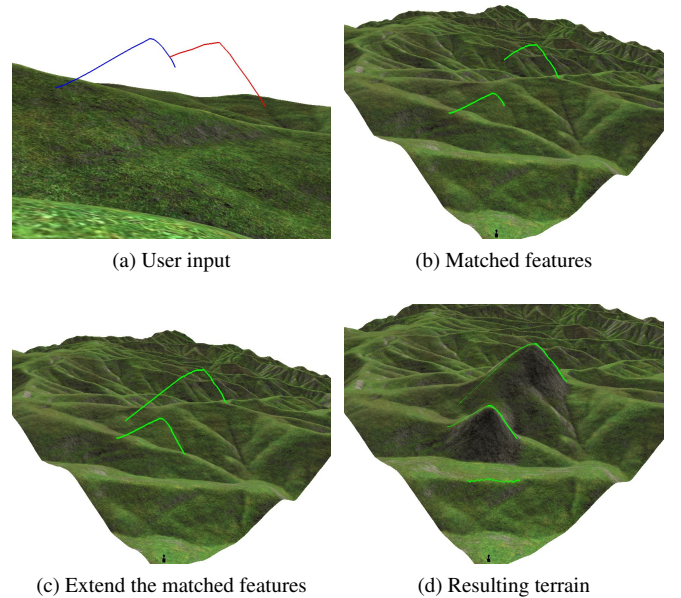


Figure 6: Completing selected features: after matching 2D strokes to terrain features, we extend these features until they reach the surface of the terrain, to ensure a smooth transition from specified silhouettes to the terrain.

501 6. Terrain deformation

502 In the previous section, we analysed terrain features and
503 used them to position the strokes in the world space. We present
504 in this section how we use them as constraints to deform the ex-
505 isting terrain.

506 6.1. Diffusion-based equation solver

507 Our deformation algorithm relies on iterative diffusion of
508 displacement constraints, which are computed from the 3D strokes
509 positioned in the world space.

510 The diffusion method, first introduced in work by Emilien
511 et al. [31], consists in computing the difference of the curve
512 height and the terrain height \mathcal{H} , and to diffuse these differences
513 (instead of absolute height values) using a multi-grid Poisson
514 solver similar that used by Hnaidi et al. [14].

515 More precisely, for each point $p = (x, y, z)$ of the stroke in
516 the world space, we compute $\delta = z - \mathcal{H}(x, y)$, and set it as a dis-
517 placement constraint. The constraints are rasterised on a grid,
518 whose resolution is equal to the terrain resolution. After hav-
519 ing set the constraints of all strokes, we perform the diffusion,
520 which gives the displacement map \mathcal{M} .

521 The displacement is finally applied on the terrain height
522 field \mathcal{H} , whose feature line silhouettes are now matching the
523 user strokes, when seen from the first-person viewpoint used
524 for sketching. The deformation only consists of adding the two
525 heights, $\mathcal{H}'(x, y) = \mathcal{H}(x, y) + \mathcal{M}(x, y)$, where \mathcal{H}' is the result-
526 ing terrain. Because height differences are propagated, instead
527 of absolute heights, the terrain preserves fine-scale details dur-
528 ing the deformation.

529 6.2. Lowering protruding silhouettes

530 After deformation, the user-defined silhouettes may be hid-
531 den by other parts of the terrain. To address this issue, we de-
532 tect the unwanted protruding silhouettes and constrain them to
533 a lower position so that the user-defined silhouettes become vis-
534 ible.

535 6.2.1. Detecting most protruding silhouette edges

536 First, all visible silhouettes are detected, with the algorithm
537 discussed in Section 5.1. These silhouettes are projected onto
538 the sketching plane. Let s be a silhouette of the deformed land-
539 scape, inherited from the example terrain. The mountain of sil-
540 houette s hides a user-specified silhouette g if s is closer to the
541 camera than g and the projection s_p of s in the sketching plane
542 has a higher altitude than g_p , the projection of g . In this case,
543 s is an unwanted protruding silhouette. Determining how much
544 s should be lowered is done as follows: Let h be the maximum
545 height difference between s and a silhouette g hidden by s . It
546 therefore follows that h is the minimum altitude by which s
547 should be lowered to ensure the silhouettes it hides become vis-
548 ible. Our solution is simply to uniformly lower s by an offset h .
549 This method is applied to all unwanted protruding silhouettes
550 and we use the set of lowered silhouettes to form new deforma-
551 tion constraints.

552 6.2.2. Updating deformation constraints

553 The new deformation constraints from the lowered protrud-
554 ing silhouettes are added to the set of constraints associated to
555 the sketched silhouettes, and the terrain is deformed once again
556 using the method of Section 6.1. This operation maintains the
557 user-specified silhouettes while lowering areas around the un-
558 wanted protruding silhouettes, so that user specifications are
559 satisfied.

560 The process of detecting protruding silhouettes and using
561 this information to further constrain the terrain is repeated un-
562 til protruding silhouettes are no longer detected. In practice, a
563 single iteration is usually sufficient to make all user-specified
564 silhouette strokes visible.

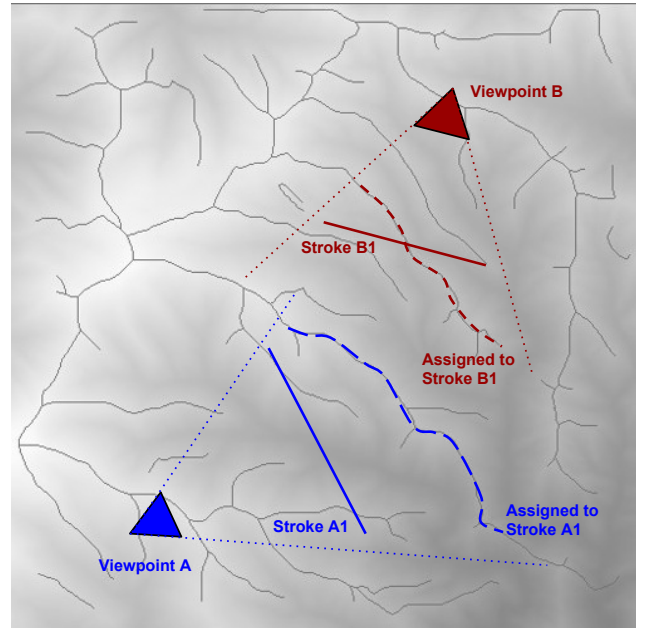


Figure 7: Multi-view from two overlapping viewpoints. Let sketch A consists of stroke A1 and sketch B consists of stroke B1. A and B are intersecting sketches since stroke B1 is visible from A and stroke A1 is visible from B. If the indicated terrain features (shown in dashed lines) are assigned to each stroke and deformed to fit the user-specified heights, then either the silhouette created by B1 will be protruding viewed from A, or the silhouette created by A1 will be protruding viewed from B. This situation can only be avoided if the section of stroke A1 visible from B has the same height values as B1.

565 7. Handling multi-view sketches

566 With respect to our earlier work [21], we improve our frame-
567 work to support multi-view sketches from different viewpoints.
568 We assume that the sketches provided by the artist do not cross
569 each other. Two sketches cross or intersect if parts of both
570 sketches are visible from the two sketching viewpoints. It would
571 be difficult to generate terrain silhouettes that match one sketch
572 and yet, are not detected as protruding from the other sketch-
573 ing viewpoint. Figure 7 shows an example of two intersecting
574 sketches. The problem of having silhouettes generated from
575 one sketch viewed as protruding silhouettes from a different
576 viewpoint cannot usually be solved, unless the intersecting sec-
577 tions have the same height values or the assigned features for

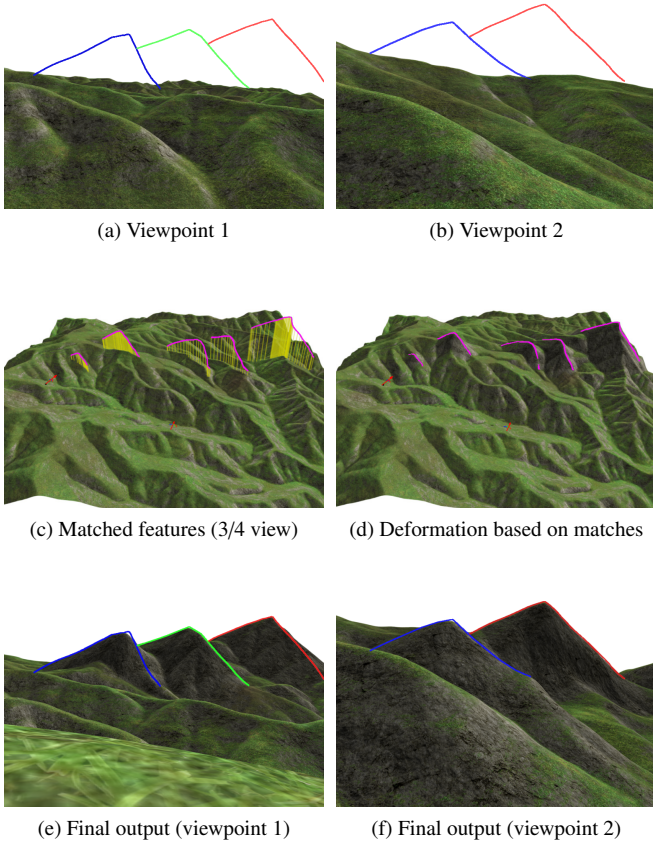


Figure 8: Sketch-based terrain editing from two different viewpoints (shown in (a) and (b)). (c) shows the terrain features assigned to each stroke, based on a modified stroke-feature matching algorithm that handles all sketches at once, while ensuring that curve constraints for different sketches do not occlude each other. The yellow lines indicate the height displacements of assigned terrain features. (d) The height displacements are used as constraints to a terrain deformation. (e,f) shows the deformed terrain from the two viewpoints. (g,h) shows the resulting terrain after lowering protruding silhouettes visible from each viewpoint.

one sketch are so far from the other sketch viewpoint that they are not visible. Thus for overlapping viewpoints that are far enough from each other, terrain features closer to the camera can be assigned such that no conflict occurs. Instead of including this additional complexity to our method, we decided not to support intersecting sketches. We argue that in the case where viewpoints are far from each other, iterative drawing can be used, since the algorithm always try to assign features that are closer to the corresponding sketch viewpoint. Iterative drawing could be used for non-intersecting multi-view sketches as well, but especially in cases where multiple viewpoints are close to each other, taking into account all the sketches when deciding the assignment of features to strokes is important. The approach discussed here provides a guarantee that each generated silhouette will fit the corresponding user strokes, with no other silhouette protruding when seen from the corresponding viewpoint.

To handle non-intersecting multi-view sketches, we first process each sketch separately by computing its stroke ordering and a list of potential terrain features for each stroke. Note that

for each sketch, we generate this list from terrain ridges and silhouettes edges detected from the sketch camera position. Once we have a priority list of candidate features for each stroke in each sketch, we run an energy minimization process that takes into consideration all the sketches at once.

The energy minimization problem (Section 5.2.2) changes as follows: for each input sketch I_i , we want to assign a terrain feature to each of its strokes s_i^j such that the total cost of all the assignments is minimized, with the additional constraint that no terrain feature assigned to a given stroke s_i^j should fall between the camera and an already assigned feature in a different sketch $I_{i'}$. This additional constraint ensures that all assigned terrain features remain visible from their respective sketch viewpoint. To handle all sketches at once in the branch-and-bound algorithm, we first explore solutions for the first drawn sketch and then proceed to the next one. Similarly to the process in Section 5.2.2, the list of candidates for every stroke is updated according to constraints within each sketch and across sketches. This modified branch and bound scheme effectively generates stroke-feature matches for all sketches.

Once we have assigned a terrain feature to each stroke, all the combined matched features are used to deform the terrain (Section 6). To handle residual artifacts from the deformation, we lower protruding silhouettes one sketch at a time, for all sketches. Because the influence of terrain deformation is localized, lowering protruding silhouettes for one sketch have a limited effect on terrain silhouettes for another sketch. Figure 8 shows a terrain editing from two sketches, each drawn from a different camera position and orientation. Note how for both sketches, user strokes correspond to terrain silhouettes, while the whole terrain remains plausible from different viewpoints. This would not have been the case if the two sketches had been processed sequentially, since deformations due to the second sketch would have likely modify silhouettes generated for the first sketch.

8. Results

Validation examples. The examples below and the associated video illustrate the results of our method in a variety of cases. In particular, Figure 9 shows editing of a terrain with a complex sketch containing 4 T-junctions. Our method is also able to handle complex mountains where ridges are not as well-defined as they are on smooth landscapes. An example of this is shown in Figure 10. Our proposed approach differs from other sketch-based methods in that non-planar silhouettes can be generated from planar user-sketched strokes. This is illustrated in Figure 11. Moreover, the method is robust enough to support terrains with few or no features, as shown in the example given in Figure 12. Indeed if the terrain contains no features, we compute a 3D embedding of stroke closest to the camera by projecting the stroke on the drawing plane determined by the camera direction and a 3D point where the stroke touches the terrain. The rest of the user strokes can then be placed in 3D with respect to the embedding of the first stroke, using the same technique we apply to strokes with no matching features in Section 5.2.2.

Fig.	Features	Matching	Deformation	Silhouettes
1	0.14	0.24	0.09	4.9
2	0.14	1.5	0.11	2.6
9	0.15	0.21	0.10	2.1
10	0.12	0.13	0.10	9.4
11	0.12	0.04	0.09	3.4

Table 1: Computation times (in seconds) for examples illustrated in this paper. We show computation times of the following steps: feature extraction, stroke-feature matching, terrain deformation, lowering protruding silhouettes.

Our complex sketch-based editing framework can be implemented at interactive rates, as illustrated in the attached video, which makes it an attractive alternative to other terrain generation/editing techniques discussed in Section 2.

Performance. The terrain editing system is implemented in C++ and the computations are measured on an Intel® Xeon® E5-1650 CPU, running at 3.20 GHz with 16 GB of memory. We present the computation times of results illustrated in this paper in the Table 1. The feature extraction and terrain deformation computation times only depend on the terrain resolution, which is 512×512 in the examples. Feature matching performance depends on the number of strokes and the number of extracted features. In our examples, the average number of extracted features was around 1000 and mostly consisted of short terrain silhouette features. The most expensive algorithm is the lowering protruding silhouettes, due to the expensive silhouette detection. Our naive implementation of silhouette detection could be optimised to significantly impact the overall performance of our algorithm. The stroke ordering algorithm has a negligible computation time. The average manual editing time was less than a minute.

Comparing feature-based constraints against planar curve constraints. Typical sketch-based terrain deformation techniques [13, 27, 15] use planar curve constraints computed from user strokes. Such planar curves can be obtained by computing the drawing plane from the user sketch and projecting strokes on this plane to obtain their 3D position in world coordinates. The normal to the drawing plane is the camera view direction and one point on this plane is obtained by computing the world coordinates of a stroke point touching the terrain. We argue that using such planar curve constraints for terrain editing produce inferior results, compared to the use of feature-based constraints. To illustrate this, we compared the two different deformation schemes, our method and the standard method, on three different inputs. Each input consists of a real landscape and a one-stroke sketch drawn from a first person perspective view (see Figure 13). Our method uses the matched terrain features obtained from Section 5 as deformation constraints. The standard method simply uses curve constraints obtained by projecting user strokes on the drawing plane. Figure 13 shows the 3D constraints used in the terrain deformation and the final terrain produced by each method. Note that the final terrain is generated by first deforming the input terrain with feature-based constraints or planar curve constraints, and then lowering pro-

truding silhouettes. In the case of planar curve constraints, this last step generates non planar silhouettes, which is already an improvement since the main pitfall of the standard method is that it produces unrealistic mountains with planar silhouettes. Even after this improvement, note how landscapes produced by the standard method have more prominent silhouettes in front of the user-specified silhouettes and thus may not reflect the user intent. This happens when a planar curve constraint is behind a terrain feature and thus the deformation raises the terrain feature making it a prominent silhouette. In contrast our proposed method is feature-aware and by generating deformation constraints based on terrain features, reduces the risk of prominent silhouettes appearing in front of user-specified silhouettes. In addition, the silhouettes we generate are non-planar, since they are matched with the depth of the associated terrain features (Figure 13(h, i)). This makes the resulting terrains look much more natural when seen from above.

User tests. We performed an informal user test on our single viewpoint system with two experienced computer artists. The system was briefly introduced to the users, who had no prior knowledge of it. They were asked to draw sketches to deform existing terrains. Both of them reported that our system was very easy to learn and use, and were able to quickly create new sceneries. Their feedback indicated that the approach is original, and seems a promising way to create a scene that matches their artistic intent. These first users also asked for the ability to move within the scene and edit the terrain from multiple viewpoints. This led to the work described in Section 7. Lastly, the users emphasised the importance of the realistic resulting terrain, and noted that it matched their sketches in the expected way.

Limitations. Although our system succeeds in matching a complex user-sketch through a natural deformation of the terrain, based on its existing features, the lack of predictability of the stroke-feature solver may be a problem. It is often not clear during the drawing stage which terrain feature will be assigned to a stroke. The artist may draw a stroke with the intention of turning a large-scale feature into a terrain silhouette, but the algorithm chooses to deform a different terrain feature instead. To address this, we could also improve our matching method using extra error functions, that take into account the placement of user strokes relative to the projection of terrain features on the drawing plane.

The editing framework is also limited in the type of strokes drawn and the type of terrain. For instance landscapes with high frequency details and a complex style such as the Grand Canyon are particularly difficult to edit since depending on the nature of the strokes and which features are assigned to strokes, the deformed region can differ significantly from the other. In general, elaborate strokes that are unlikely to be terrain silhouette, except from a specific viewpoint, often cause several iterations of terrain deformation in the neighbourhood of the assigned features, that either do not succeed in removing all protruding silhouettes or look unrealistic when viewed from a different viewpoint.

751 Another limitation comes from our deformation solver. The
 752 diffusion-based deformation method sometimes creates small
 753 declivities around the extremity of a constraint curve, when the
 754 slope of the curve is high and the extremity is located on the
 755 terrain: in this case, the terrain locally inflates, except at this
 756 end-point where the deformation is zero, which causes the problem.
 757 Using an inverse distance to deform a terrain [32] does not
 758 work either, because of our use of curves as constraints. Future
 759 work still needs to be done on terrain deformation, especially
 760 for curve-based deformations.

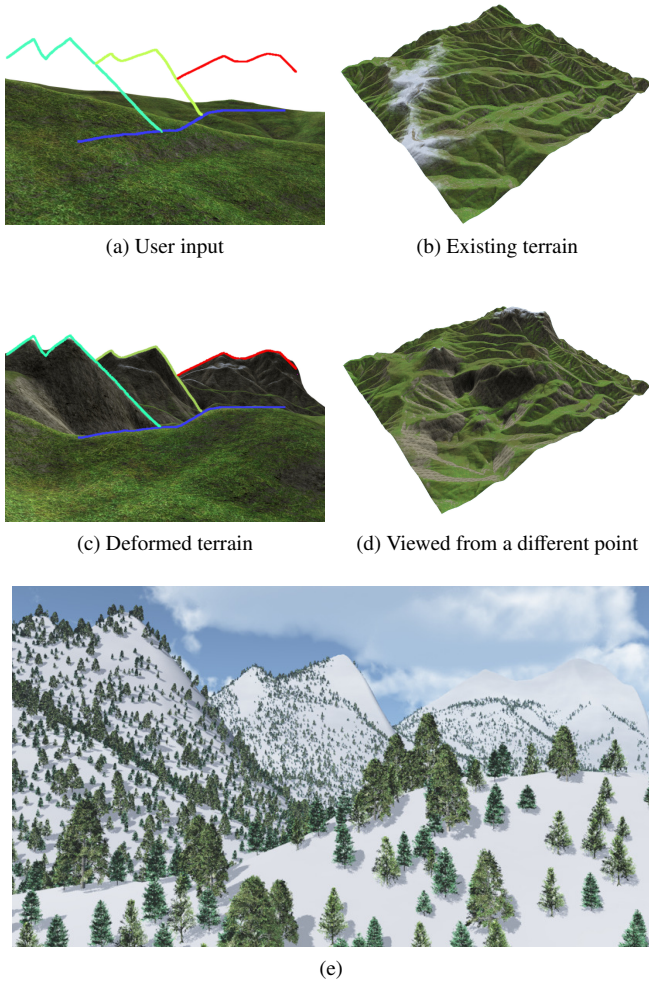


Figure 9: Terrain editing from a complex user sketch.

761 9. Conclusion

762 We presented a sketch-based modelling method enabling
 763 the deformation of a terrain from a single viewpoint, and then
 764 extended it to handle multiple viewpoints simultaneously. The
 765 user sketches a few silhouette strokes forming a graph with
 766 T-junctions, similar to the silhouette representations used in
 767 artistic terrain sketching. A key feature of our method is that
 768 sketched silhouettes are matched with existing terrain features:
 769 this enables our technique to both match silhouette strokes with

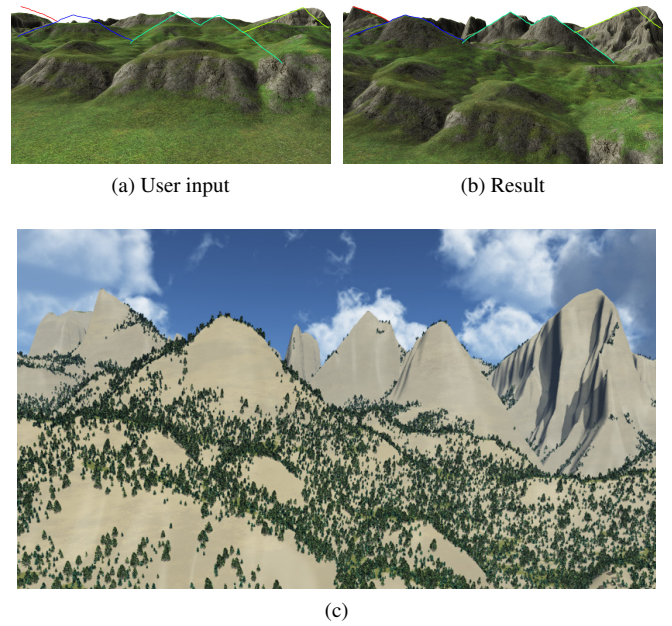


Figure 10: Editing a complex rocky mountain from a complex sketch.

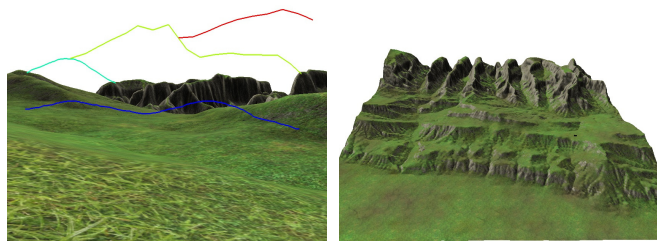
770 a non-planar curve, and produce a deformation that does not
 771 spoil plausibility, since the structure of ridges and valleys typi-
 772 cally remains unchanged.

773 Acknowledgements

774 This work was conducted during an internship of Flora Pon-
 775 jou Tasse at Inria Rhône-Alpes in Grenoble. It was partly sup-
 776 ported by the ERC advanced grant EXPRESSIVE.

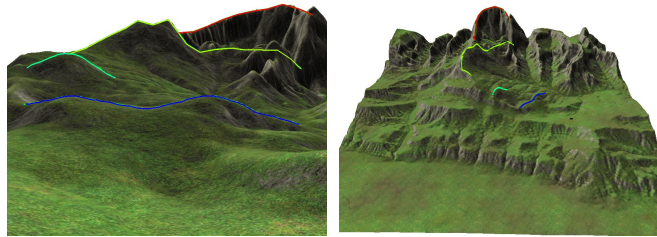
References

- [1] Fournier A, Fussell DS, Carpenter LC. Computer rendering of stochastic models. *Communications ACM* 1982;25(6):371–84.
- [2] Miller GSP. The definition and rendering of terrain maps. *SIGGRAPH Comput Graph* 1986;20(4):39–48.
- [3] Lewis JP. Generalized stochastic subdivision. *ACM Trans Graph* 1987;6(3):167–90.
- [4] Musgrave FK, Kolb CE, Mace RS. The synthesis and rendering of eroded fractal terrains. In: *Proceedings of the 16th Annual Conference on Computer Graphics and Interactive Techniques. SIGGRAPH '89*; New York, NY, USA: ACM; 1989, p. 41–50.
- [5] Roudier P, Peroche B, Perrin M. Landscapes synthesis achieved through erosion and deposition process simulation. *Computer Graphics Forum* 1993;12(3):375–83.
- [6] Chiba N, Muraoka K, Fujita K. An erosion model based on velocity fields for the visual simulation of mountain scenery. *Journal of Visualization and Computer Animation* 1998;9(4):185–94.
- [7] Nagashima K. Computer generation of eroded valley and mountain terrains. *Visual Computer* 1997;13(9-10):456–64.
- [8] Neidhold B, Wacker M, Deussen O. Interactive physically based fluid and erosion simulation. *Natural Phenomena* 2005;;25–32.
- [9] Kristof P, Benes B, Krivanek J, Stava O. Hydraulic erosion using smoothed particle hydrodynamics. *Computer Graphics Forum* 2009;28(2):219–28.
- [10] Cohen JM, Hughes JF, Zeleznik RC. Harold: A world made of drawings. In: *Proceedings of the 1st International Symposium on Non-photorealistic Animation and Rendering. NPAR '00*; New York, NY, USA: ACM; 2000, p. 83–90.



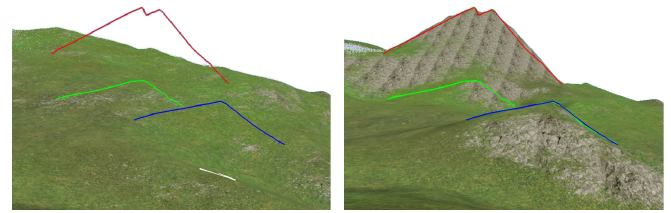
(a) User input

(b) Existing terrain



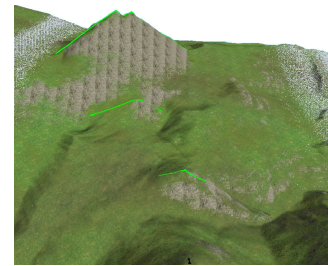
(c) Deformed terrain

(d) Result viewed from a different point



(a) User input

(b) Result



(c) View from another point

Figure 11: Terrain editing produces non-planar silhouettes in the output, from 2D planar strokes.

Figure 12: Adding deformation constraints automatically: the stroke furthest away from the user did not have an assigned feature to it and so one was automatically generated, and positioned on a plane orthogonal to the view direction, such that stroke ordering is respected.

- [11] Watanabe N, Igarashi T. A sketching interface for terrain modeling. In: ACM SIGGRAPH 2004 Posters. SIGGRAPH '04; New York, NY, USA: ACM; 2004, p. 73–.
- [12] Zhou H, Sun J, Turk Gbb, Reh Gbb. Terrain synthesis from digital elevation models. *IEEE Transactions on Visualization and Computer Graphics* 2007;13(4):834–48.
- [13] Gain J, Marais P, Straer W. Terrain sketching. In: Proceedings of I3D 2009: The 2009 ACM SIGGRAPH Symposium on Interactive 3D Graphics and Games. 2009, p. 31–8.
- [14] Hnaidi H, Guerin E, Akkouche S, Peytavie A, Galin E. Feature based terrain generation using diffusion equation. *Computer Graphics Forum* 2010;29(7):2179–86.
- [15] Tasse F, Gain J, Marais P. Enhanced texture-based terrain synthesis on graphics hardware. *Computer Graphics Forum* 2012;31(6):1959–72.
- [16] Genevaux JD, Galin E, Guerin E, Peytavie A, Benes B. Terrain generation using procedural models based on hydrology. *ACM Transactions on Graphics* 2013;32(4).
- [17] Dos Passos V, Igarashi T. Landsketch: A first person point-of-view example-based terrain modeling approach. In: Proceedings - Sketch-Based Interfaces and Modeling, SBIM 2013 - Part of Expressive 2013. 2013, p. 61–8.
- [18] Karpenko O, Hughes J. Smoothsketch: 3d free-form shapes from complex sketches. In: ACM SIGGRAPH 2006 Papers, SIGGRAPH '06. 2006, p. 589–98.
- [19] Singh K, Fiume E. Wires: A geometric deformation technique. In: Proceedings of the 25th Annual Conference on Computer Graphics and Interactive Techniques. SIGGRAPH '98; New York, NY, USA: ACM; 1998, p. 405–14.
- [20] Zimmermann J, Nealen A, Alexa M. Silsketch: Automated sketch-based editing of surface meshes. In: Proceedings of the 4th Eurographics Workshop on Sketch-based Interfaces and Modeling. SBIM '07; New York, NY, USA: ACM; 2007, p. 23–30.
- [21] Tasse FP, Emilien A, Cani MP, Hahmann S, Bernhardt A. First person sketch-based terrain editing. In: Proceedings of the 2014 Graphics Interface Conference. GI '14; Canadian Information Processing Society; 2014, p. 217–24.
- [22] Natali M, Lidal EM, Viola I, Patel D. Modeling terrains and subsurface geology. In: Proceedings of EuroGraphics 2013 State of the Art Reports (STARs). Eurographics; Eurographics 2013 - State of the Art Reports; 2013, p. 155–73.
- [23] Mandelbrot BB. *The fractal geometry of nature*. New York: W. H. Freeman; 1983.
- [24] Ebert DS, Musgrave FK, Peachey D, Perlin K, Worley S. *Texturing and Modeling: A Procedural Approach*. 3rd ed.; San Francisco, CA, USA: Morgan Kaufmann Publishers Inc.; 2002.
- [25] Kelley AD, Malin MC, Nielson GM. Terrain simulation using a model of stream erosion. *Computer Graphics (ACM)* 1988;22(4):263–8.
- [26] McCrae J, Singh K. Sketch-based path design. In: Proceedings of Graphics Interface 2009. GI '09; Toronto, Ont., Canada, Canada: Canadian Information Processing Society; 2009, p. 95–102.
- [27] Bernhardt A, Maximo A, Velho L, Hnaidi H, Cani MP (IMPA, Rio de Janeiro, Brésil). Real-time Terrain Modeling using CPU-GPU Coupled Computation. In: XXIV SIBGRAPI. Maceio, Brazil; 2011,.
- [28] Chang YC, Sinha G. A visual basic program for ridge axis picking on dem data using the profile-recognition and polygon-breaking algorithm. *Computers and Geosciences* 2007;33(2):229–37.
- [29] Bangay S, de Bruyn D, Glass K. Minimum spanning trees for valley and ridge characterization in digital elevation maps. In: Proceedings of the 7th International Conference on Computer Graphics, Virtual Reality, Visualisation and Interaction in Africa. AFRIGRAPH '10; New York, NY, USA: ACM; 2010, p. 73–82.
- [30] Clausen J. Branch and bound algorithms-principles and examples. *Parallel Computing in Optimization* 1997;:239–67.
- [31] Emilien A, Poulin P, Cani MP, Vimont U. Interactive procedural modeling of coherent waterfall scenes. *Computer Graphics Forum* 2014;To appear.
- [32] Jenny H, Jenny B, Cartwright WE, Hurni L. Interactive local terrain deformation inspired by hand-painted panoramas. *Cartographic Journal*, The 2011;48(1):11–20.

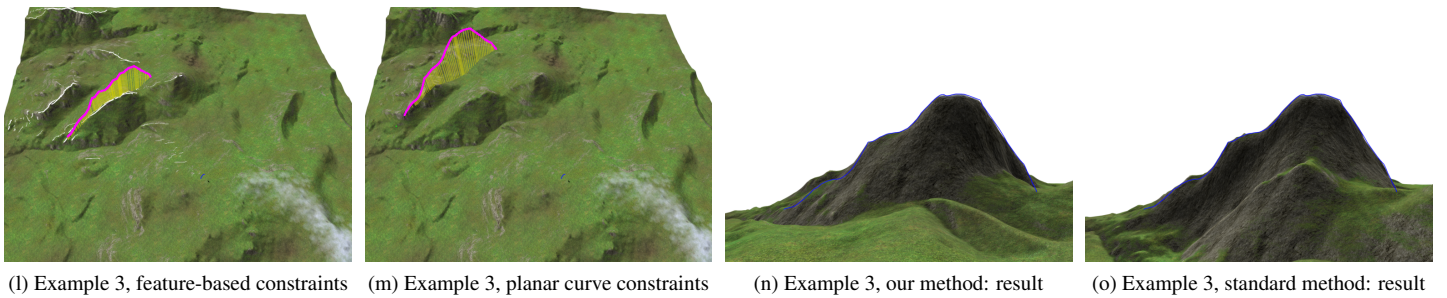
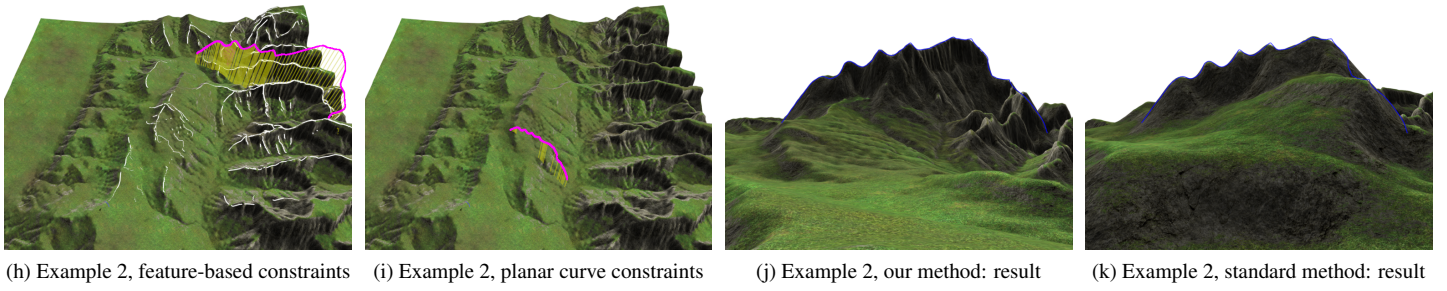
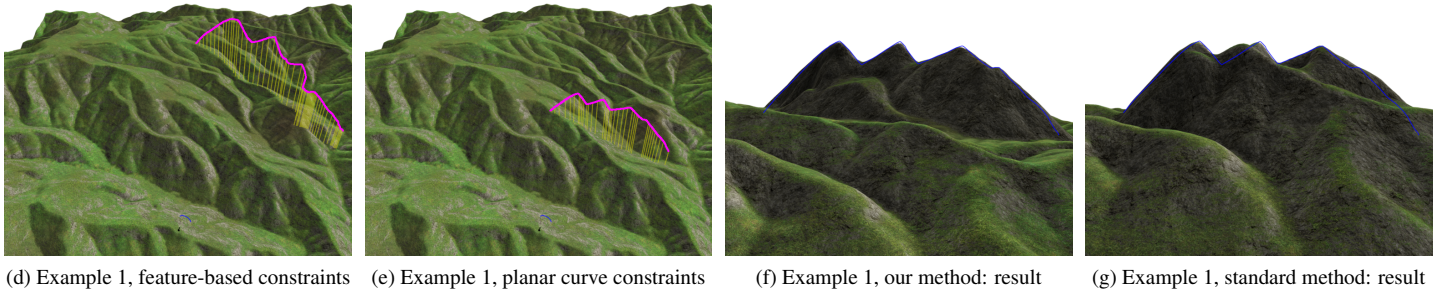
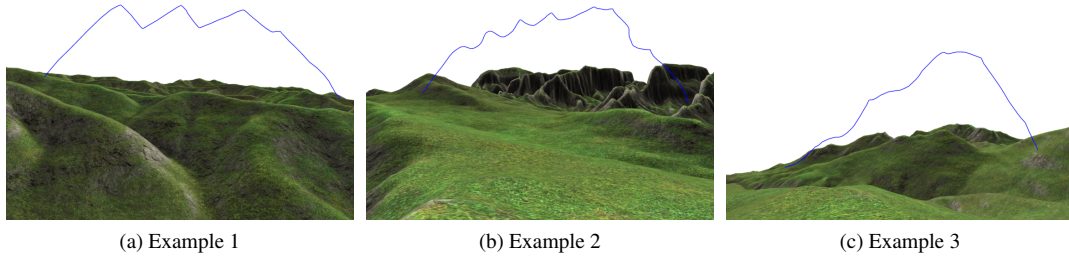


Figure 13: Comparing terrain deformation with feature-based constraints (our method) against editing from planar curve constraints (standard method). The final output produced by our deformation scheme has less prominent terrain silhouettes appearing between the camera position and the user-specified silhouettes, and thus is closer to the user intent.